Thesis for the Degree of Master of Engineering

Non-destructive and Non-invasive Elasticity Measurement of Tissue Engineering Scaffold Using Ultrasound

By

Chulhee Yun

Interdisciplinary Program of Biomedical Mechanical & Electrical Engineering

College of Engineering

Pukyong National University

February 2019

Non-destructive and Non-invasive Elasticity Measurement of Tissue Engineering Scaffold Using Ultrasound

초음파를 이용한 조직공학 세포지지체의 비파괴적 비침습적 탄성 측정

Advisor: Prof. Seung Yun Nam

by

Chulhee Yun

A thesis submitted in partial fulfillment of the requirement

for the degree of

Master of Engineering

in Interdisciplinary Program of Biomedical Mechanical & Electrical Engineering

College of Engineering

Pukyong National University

February 2019

Non-destructive and Non-invasive Elasticity Measurement of Tissue Engineering Scaffold Using Ultrasound

A dissertation

by

Chulhee Yun

Approved by:

_____

(Chairman)

_____ _____

(Member) (Member)

February 22, 2019

초음파를 이용한 조직공학 세포지지체의 비파괴적 비침습적 탄성 측정

윤 철 희

부경대학교 대학원 의생명기계전기융합공학협동과정

요 약

조직공학용 세포지지체의 물성은 생체적합성과 세포의 거동 및 기능에 큰 영향을 준다. 이러한 세포지지체의 기계적 특성을 측정하는 기존의 방법들은 대부분 지지체의 파괴적 과정을 거치게 되며 동일 지지체내의 물성변화를 장기간 계속 측정할 수 없는 제한이 있었다. 하지만, 실제 피부 질병 진단 등에 사용되어 온 표면 탄성파 측정법과 전단 탄성영상법을 이용하면 점탄성을 가지는 세포지지체의 비파괴적 물성측정이 가능하다.

본 연구에서는 세포지지체 물성 변화의 비파괴적인 측정을 위해 빔포밍을 이용한 집속 초음파 및 소프트웨어 기반의 초고속 영상법을 이용하여 실제 조직공학용 세포지지체와 유사한 기계적 특성을 가지는 다양한 물성의 젤라틴 기반 샘플 및 레이저를 조사하여 점탄성을 조절할 수 있는 알긴산-금나노입자 기반 세포지지체를 제작하여 표면 탄성파의 전파를 시뮬레이션하고 이를 레오미터 측정치와 비교 분석하였다. 또한, 전단 탄성영상법을 이용하여 얇은 조직공학 세포지지체를 측정할 때 표면 탄성파의 영향으로 탄성도 측정이 어려운 구역을 영상처리기술인 상호 상관을 최적화하여 기계적 특성을 측정하였다.

Table of contents

List of table

List of figure

1. Introduction

1.1. Tissue engineering

Tissue engineering aims to improve or replace the structure and function of deteriorated tissue using substitutes or scaffolds fabricated of various biomaterials that can grow with damaged tissue.[1, 2] The general principle of tissue engineering combine living cells/tissues, biomaterials scaffolds and growth factors/bioreactors and are therefore integrated and have expertise in the relevant fields of clinical medicine, mechanical engineering, materials science, genetics and life sciences as shown in

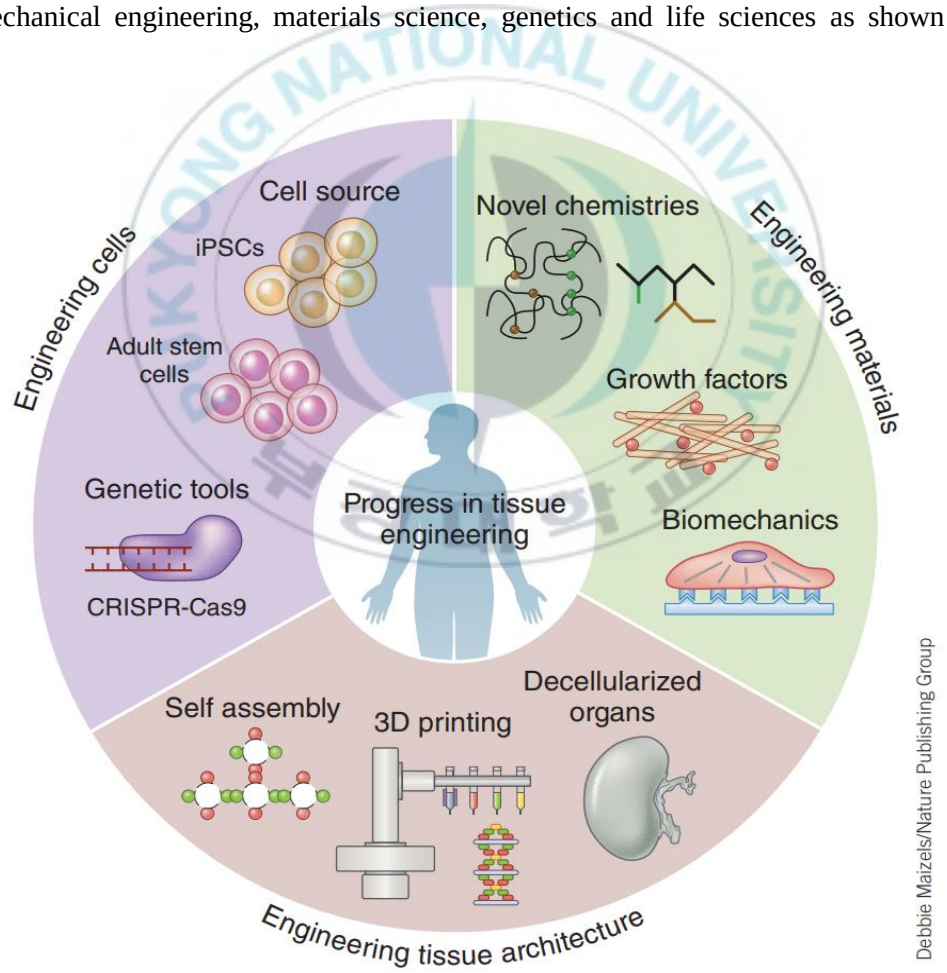

Figure 1. Summary of tissue engineering progress in the past decade.[2]

Figure 1.[3] In particular, mechanical properties of tissue-engineered substitutes needs to be comparable with that of native or surrounding tissue and are one of the most important factors to be monitored because they can significantly affect the biocompatibility, biodegradability, cell behaviors and functions.[4, 5] Therefore, tissue engineering applications need a suitable range of mechanical properties for the tissue-engineered scaffolds to have the native tissue or organ mechanical property, and to be able to avoid the side effects resulting from the stress-shielding mechanism.[6] Accordingly, conventional methods including rheological characterization and tensile strength tests have been widely used to assess the mechanical properties of the tissue-engineered constructs. However, the conventional methods for the assessment of the mechanical properties are mostly destructive and can hardly be used continuously in clinical and in-vivo models.[7] To overcome these limitations and measuring the shear modulus quantitatively with a higher contrast ratio than bulk modulus (Figure 2), shear wave elasticity imaging (SWEI) and acoustic surface wave have been recently applied to various tissue engineering applications.[8, 9]

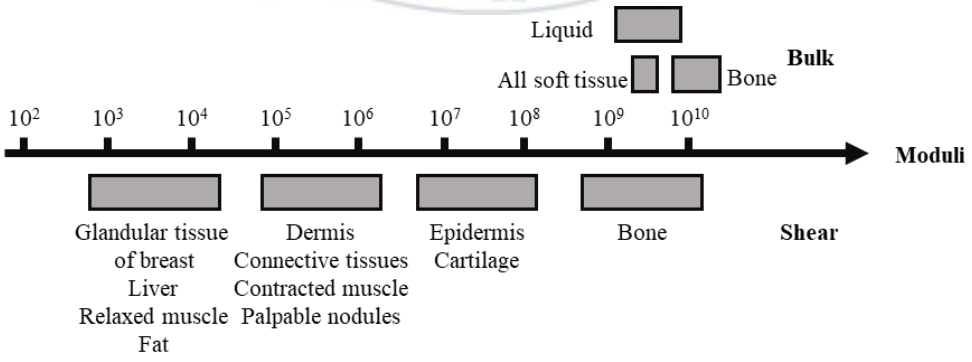

Figure 2. Summary of the variation of shear modulus and bulk modulus for various materials and body tissues.

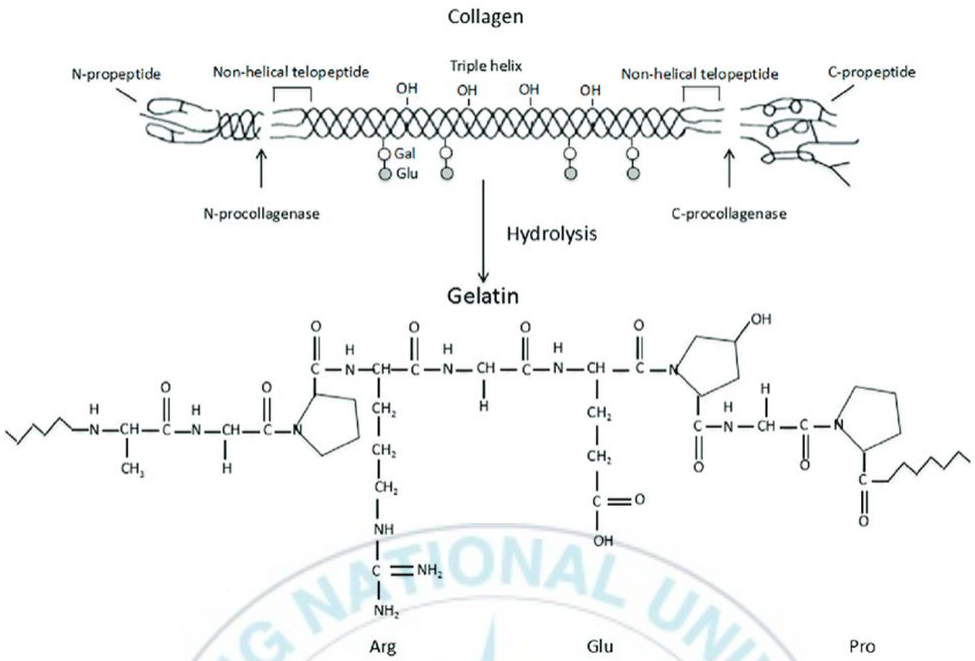

Figure 3. Schematic description of the collagen hydrolysis to gelatin.[11]

In this study, gelatin and collagen were mainly used for tissue engineering applications. Gelatin can be obtained by controlled hydrolysis of collagen, a fiber-insoluble protein, which is generally seen in nature and is the main component of skin, bone and connective tissue.[10] Gelatin is a kind of protein and composed in a unique order of amino acids. Although gelatin is 98–99% protein by dry weight, the characteristic property of gelatin is the high content of amino acids such as glycine, proline, hydroxyproline, glutamic acid, alanine and arginie.[11] Structurally, the molecules of gelatin are X and Y, in many cases proline and hydroxycurulin contains gelatin and a repetitive sequences of glycine-YX triplet which is a triplet structure of water. This sequence is responsible for the gel helix structure and the ability to form a gel in which spiral domains are formed in the protein chain of gelatin that immobilizes water. The purification type collagen, gelatin is used in a variety of biomedical applications as

scaffolds, plasma expanders, wound dressings, adhesives and surgical absorbent pads. Collagen, also known for its broad range of biomedical uses, is known to express antigens in physiological conditions, but not gelatin-like antigenicity.[12]

The surface of scaffolding materials, degradation rate and biodegradability are generally required for a tissue engineering scaffold material. Because the surface of the tissue engineering scaffold can directly affect cellular response and ultimately the tissue regeneration.[13] Gelatin and collagen are less expensive molecules as well as a broader biodegradability for well-accepted biocompatibility and are also used in the surface modification techniques.[14] Therefore, gelatin is frequently used for fabrication of tissue engineering scaffold and is mainly used for mimicking the tissue-engineered scaffolds in this paper.

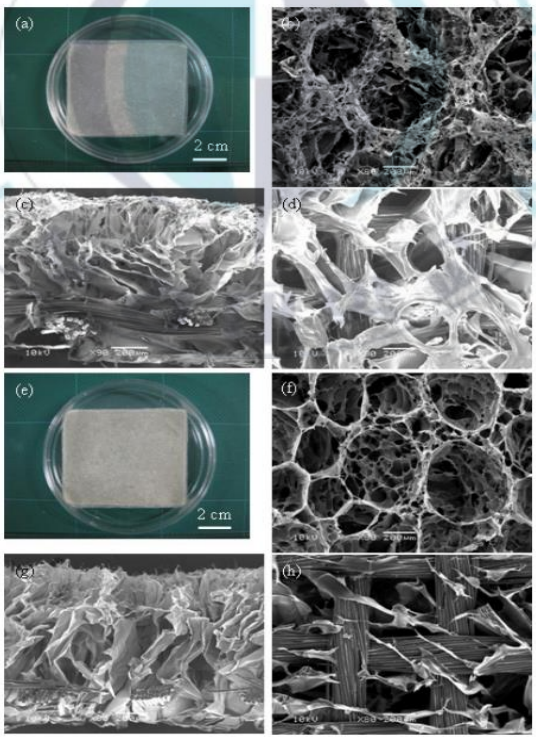

Figure 4. PLLA–collagen (a–d) and PLLA–gelatin (e–h) hybrid scaffolds.[13]

1.2. Shear wave elasticity imaging

Ultrasonic elasticity imaging has been investigation since the late 1990's for studying the mechanical properties of the tissue, which can associate with the progress of the fibrotic tissues and scaffolds or increasing of the tissue cellular density as can occur with inflammation, malignant tumors and other various cancers.[15] Recently, the software and hardware of the ultrasound systems have been improved and numerous clinical applications of ultrasonic elasticity imaging for the assessment of mechanical property have been reported to replace manual palpation of clinicians diagnose and monitor diseases non-invasively and non-destructively based on stiffness contrast between the normal tissues and abnormal tissues.[16] Therefore, various methods of ultrasonic elasticity imaging have been studied for many years including acoustic radiation force impulse imaging, shear wave elasticity imaging, supersonic shear

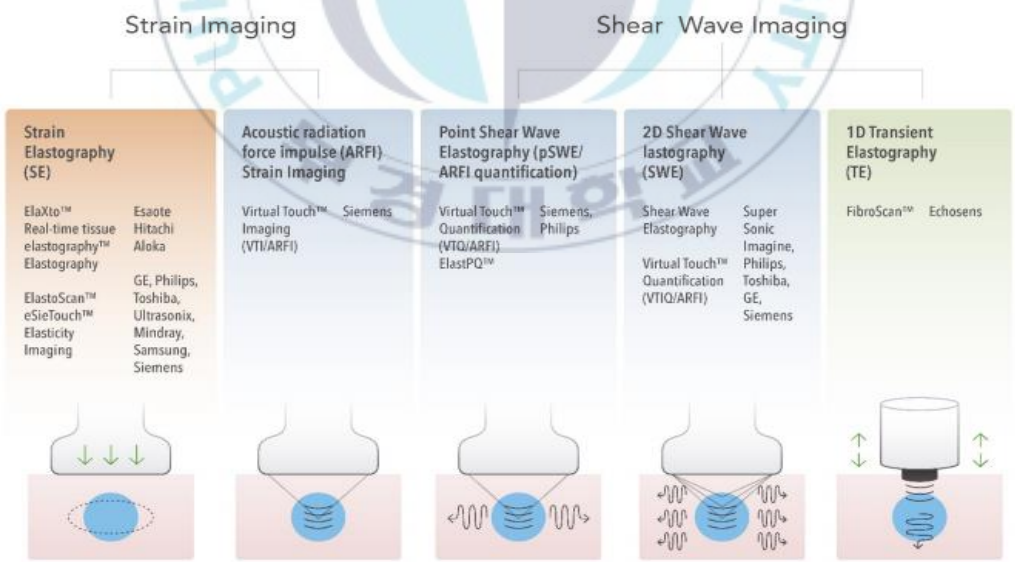

Figure 5. Ultrasonic elasticity imaging techniques.[17]

imaging, shear wave spectroscopy, comb-push ultrasound shear elastography, and spatially modulated ultrasonic radiation force imaging.[17]

SWEI can quantify the elasticity and image the structure of the target region, based on the evaluation of radio frequency (RF) echo signal and relation that shear wave propagation speed is proportional to the stiffness of the material. Because shear waves can be generated by a radiation force of a focused acoustic impulse, SWEI can non-destructively and continuously monitor changes in tissue stiffness.[18] The SWEI enables quantitative assessments of tissue viscoelasticity, thereby it can be a useful tool for numerous preclinical and clinical approaches such as diagnosis of tissue abnormalities and monitoring of scaffold degradation at various time points.[19] However, SWEI can easily suffer from the strong ultrasonic signals at the surface where multiple reflections can occur due to the differences in acoustic impedances, which can

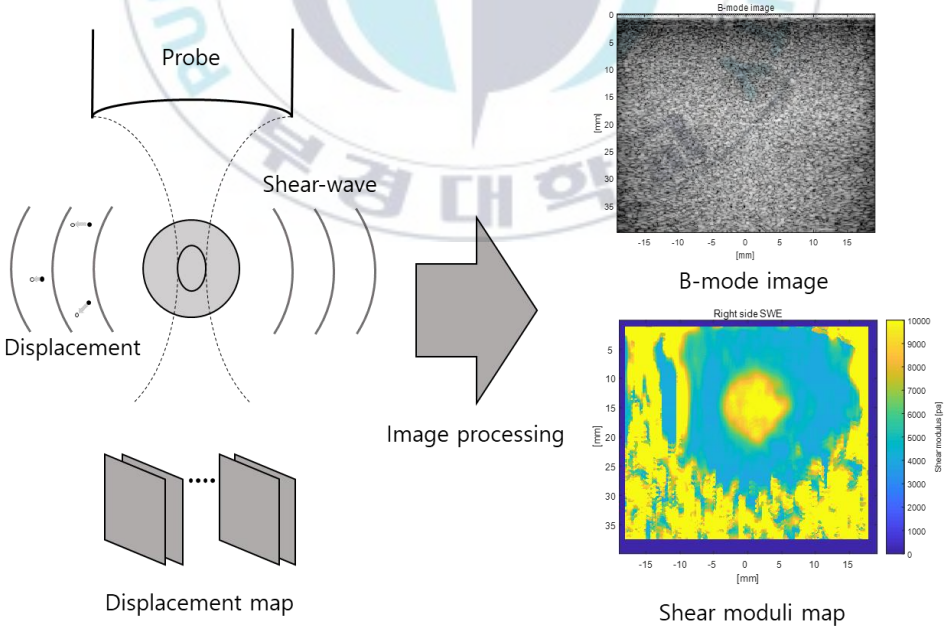

Figure 6. The experimental procedures and results of shear wave elasticity imaging.

considerably restrict its potential use in tissue characterization often applied in superficial tissue regions.[20]

Therefore, in this study, optimized parameters in post-processing of SWEI were explored to accurately assess shear modulus of the gelatin based tissue-engineered phantom with reduced effects of acoustic surface waves in the superficial regions. In previous studies, SWEI is reported to measure the mechanical property of various tissue-engineered scaffolds. However, no reported resulted are found in improvement of acoustic surface wave effects for SWEI in superficial regions of tissue engineering models. To be specific, data processing related to cross-correlation was optimized for precise evaluation of shear wave propagation speeds based on monitoring of the quantification errors in SWEI measured in tissue-mimicking models.

1.3. Acoustic surface wave assessment

In order to apply the SWEI to the mechanical property evaluations of the tissue-engineered scaffolds, a material of acoustic scattering such as silica should be added in the scaffolds for tracking the particle motions and calculating the displacements. However, acoustic scattering materials can change the mechanical properties of the tissue-engineered scaffolds and cell behavior. Therefore, acoustic surface waves have been applied to measure the overall elasticity of a medium without scattering materials by applying the characteristics of ultrasonic waves in which ultrasonic signals are strongly generated due to reflection of ultrasonic signals between materials having different acoustic impedances in the ultrasound image. As shown in Figure 5, since the shear waves are generated and spread in the medium, the mechanical properties inside

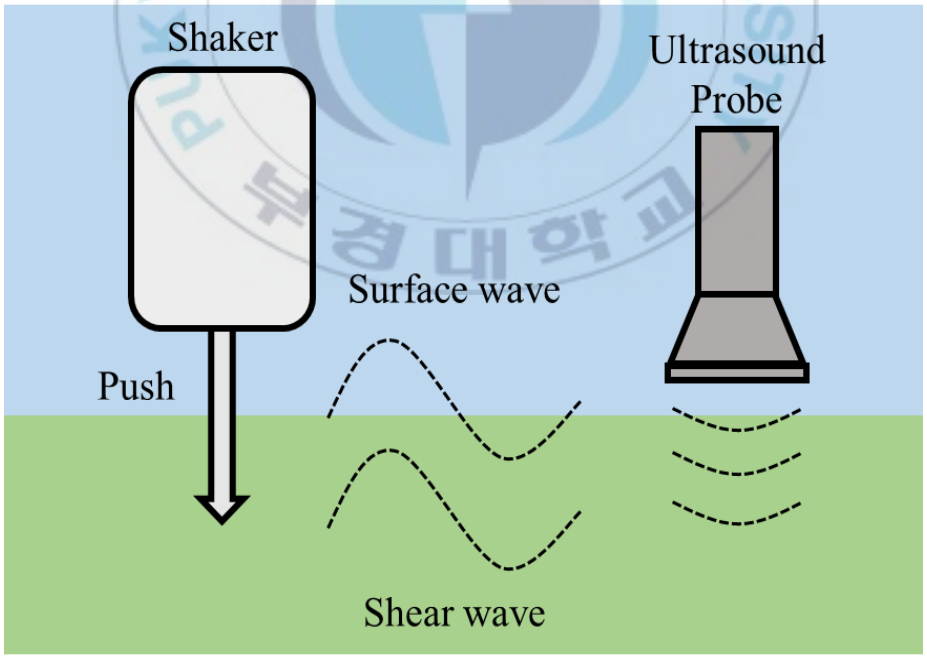

Figure 7. The difference of the surface wave and shear wave for measuring the elasticity.

the medium can be measured. On the other hand, surface waves are generated from the surface of the medium, the overall mechanical properties of the medium can be measured. Wherefore, acoustic surface wave assessments are used to measure the non-destructive properties of viscoelastic tissue-engineered scaffolds without the additional scattering materials required in the SWEI.[21] Although the acoustic surface wave can only generate on the surface of a target region, the optical method is the more diffuse reflection that can experience difficulties due to the cause of phase distortion from the

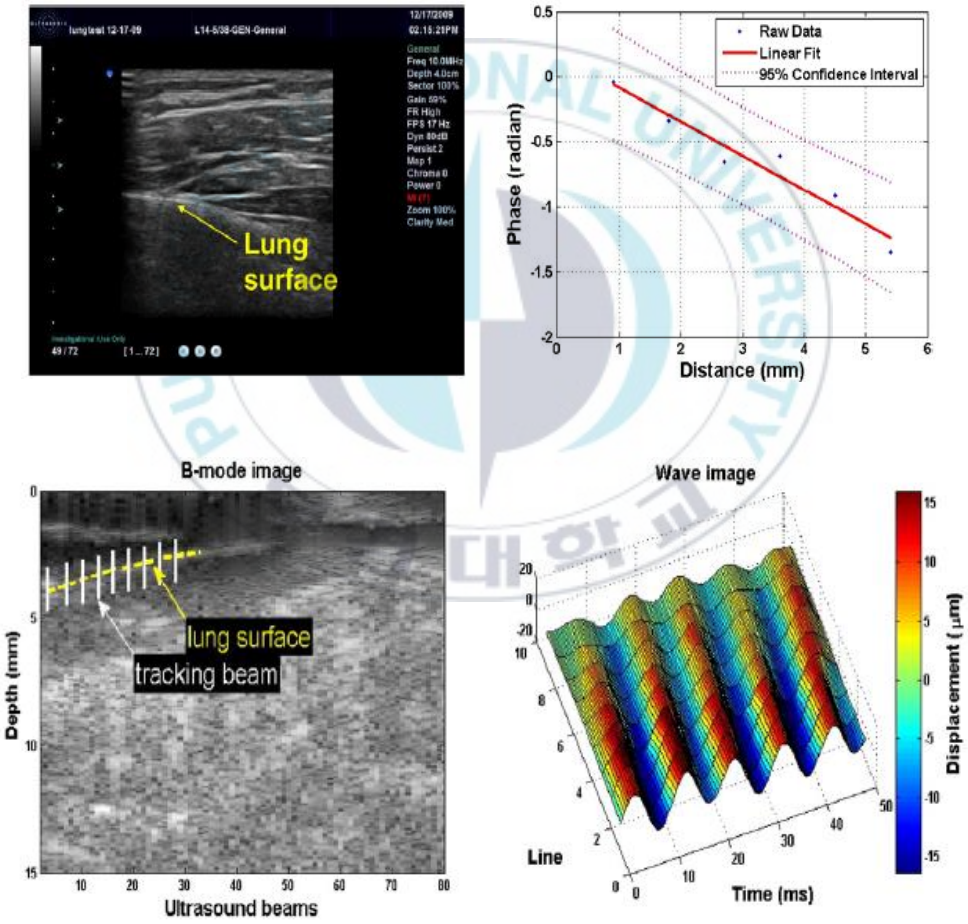

Figure 8. Measurement of human lung applying the acoustic surface wave.[23]

optical scattering coefficient of the biomedical materials is mostly over 10 times larger than their absorption coefficient.[22]

Measurement of the acoustic surface wave velocity is a discovery of the target surface as multiple time points for detecting the propagation of surface Rayleigh waves, surface waves and measuring the shear modulus similar to SWEI. Acoustic surface wave has been reported substantially in various biomedical applications, such as tissue engineering, skin, lung and artery.[23]

In this paper, we have used the Matlab based ultrasonic simulation tool, K-wave, to verify the non-destructive assessment of tissue-engineered scaffolds using acoustic surface waves. In addition, based on the simulation results, acoustic surface wave measurements of various concentrations gelatin based scaffolds and were measured by ultrafast ultrasound imaging method. Also, results from acoustic surface wave assessments are compared with the measured value by a rheometer, which is a conventional mechanical properties measuring method, to confirm the validity of the measurement of acoustic surface wave.

2. Materials and methods

2.1. Fabrication of tissue-mimicking phantom for SWEI

A tissue-mimicking phantom with the size of 10 × 10 × 0.8 cm^3 was fabricated using gelatin (Sigma Co., St. Louis, USA) and psyllium hydrophilic mucilloid fibers (sugar-free Metamucil®, OH, USA) for the superficial tissue-engineered scaffolds.[24] Gelatin was frequently used for fabrication of tissue engineering scaffold. Psyllium hydrophilic mucilloid fibers were added into the tissue-engineered scaffold to fabricate the recommended backscatter coefficient to mimic the construction of soft tissues and generate speckle patterns in ultrasound images. Psyllium hydrophilic mucous fibers at 2 wt.% were added 6 wt.% gelatin to make homogeneous tissue-mimicking phantom to perform SWEI in a superficial tissue engineering model.

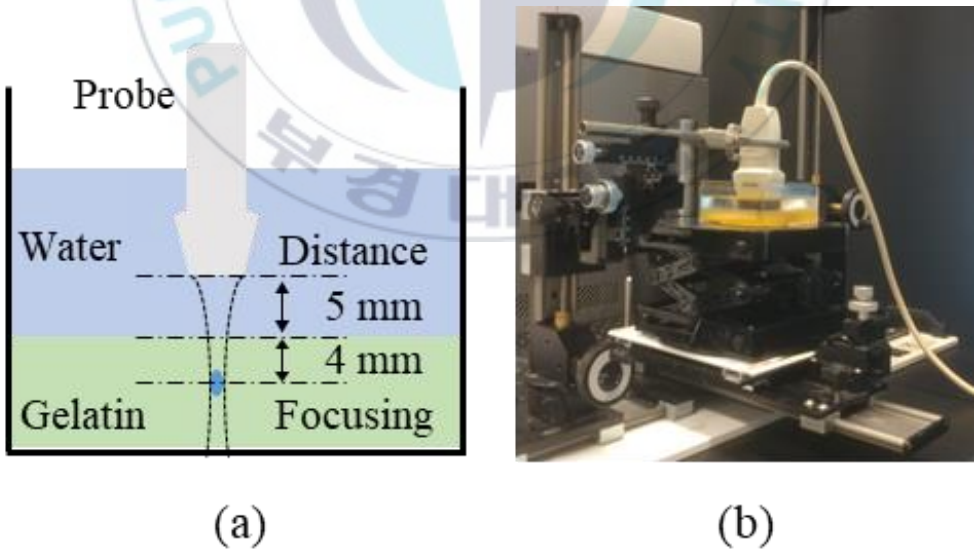

Figure 9. (a) Graphical representation of the focusing depth, distance between the probe and the phantom surface. (b) The experimental setup of shear wave elasticity imaging.

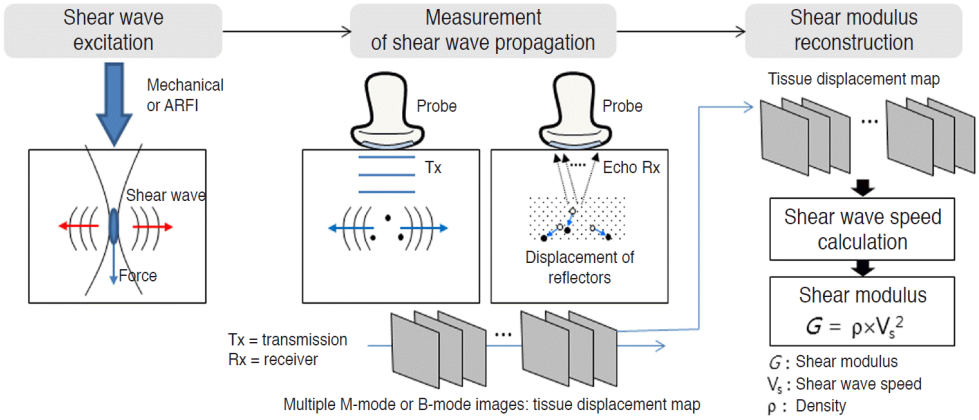

Figure 10. Diagram depicting the process of ultrasound image based shear wave elasticity imaging.[25]

2.2. Shear wave elasticity imaging

The ultrafast ultrasound imaging was performed with a programmable ultrasound data acquisition system (Vantage 128, Verasonics Inc., Kirkland, WA, USA) using a linear array transducer (L7-4, Philips Healthcare, Andover, MA, USA). In order to track the shear wave, ultrafast ultrasound imaging was performed to extract more images than conventional ultrasound images within the same time. Furthermore, to perform non-destructive and non-invasive SWEI through an acoustic radiation force impulse (ARFI), an ultrasonic probe was used to perform beamforming for focusing followed by simultaneous ultrasound B-mode imaging. The approximate SWEI procedure is shown in Figure 10.[25] The tissue-mimicking phantom was immersed in water and located at 5 mm below the transducer to avoid the near field effects in ultrasonic beamforming as shown in Figure 9. The ultrasound push beam was transmitted at a depth of 4 mm below the surface of the phantom for 500 μs using 16 elements of the array transducer with a center frequency of 4 MHz. Subsequently, 100 frames were acquired in a pulse

repetition interval of 100 μs (i.e., at 10 kHz) using 128 elements at a center frequency of 6.5 MHz.

The acquired ultrasound B-mode data after ultrasonic pushing was post-processed using a two-dimensional auto-correlation based method to estimate the motion induced from the shear waves over time.[26] Auto-correlation is the correlation of signal delay or proprietary delayed copy and shows similarity between observations as a function of delay time. On the sequence of the estimated particle velocity, cross-correlation was used to calculate the propagation time between two distinct shear wave profiles at different lateral locations defined by a respective window size.[27] Furthermore, as shown in Figure 10, the final shear wave propagation speed at a point of interest was calculated by averaging the values at 3 lines (A, B and C). The respective axial and lateral distances were estimated according to the window sizes of 2, 4, 6, and 8 with a unit size of 0.115 mm in the axial direction and 0.149 mm in the lateral direction in the particle velocities maps. The ultrasound wavelength was 0.237 mm. After applying the cross-correlated values, the shear wave propagation speed (V_s) was calculated as equation (1)[28]

$$V_s = \sqrt{V_a^2 + V_l^2} \qquad (1)$$

where V_a and V_l are shear wave propagation velocities in axial and lateral directions, respectively. The shear modulus (G) can be calculated with the estimated shear wave speed using equation (2)

$$\mathrm{G} = \rho V_s^2 \qquad (2)$$

where ρ is the material density. The shear moduli maps were created based on the calculated modulus at each point in the target regions.

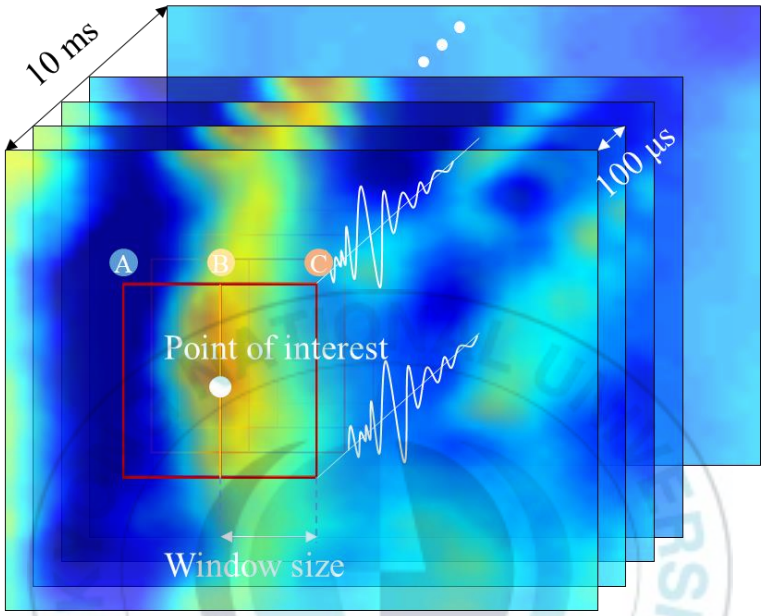

Figure 11. Diagram of the calculation of cross-correlation at a point of interest in a window using particle velocity maps.

2.3. Fabrication of tissue-mimicking phantom for acoustic surface wave

In order to make a similar intensity of human skin model, 3 %, 6 %, 9 % and 12 % of porcine skin gelatin powder (Sigma Co., St. Louis, USA) were used to make scaffolds. The reason that the concentration of gelatin differs is that shear modulus varies depending on concentration, which means that the mechanical properties differ in tissue engineering. The gelatin powder weighed according to the concentration was added to a beaker containing distilled water, mixed with a steer bar and heated to 60 ° C due to the gelatin is soluble in hot than in cold water. When all the materials were dissolved, in order to equalize physical properties that are important indicators in tissue engineering and to prevent scattering owing to air bubbles in ultrasound images, air bubbles were removed by using a vacuum chamber. After that, it was poured into a pre-prepared frame and left at 4 ° C for 6 hours. Since the gelatin scaffold varies in physical properties with temperature, the gelatin scaffold was exposed to room temperature for a certain period of time before the experiment.

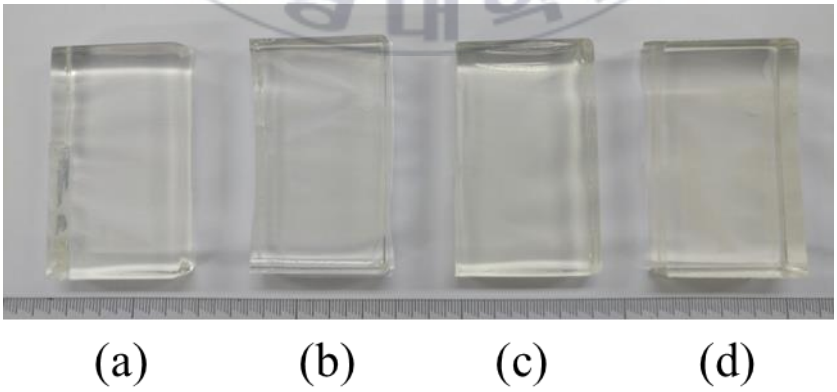

Figure 12. (a) 3%, (b) 6%, (c) 9% and (d) 12% gelatin tissue-mimicking phantom photograph for acoustic surface wave and rheometer measurement.

2.4. Fabrication of alginate-gold nanoparticle based tissue-engineered scaffolds

A liposome containing gold nanoparticles and calcium was prepared using high concentration of $CaCl^2$ encapsulated by interdigitation fusion method and fused with alginic acid to prepare alginate-gold nanoparticle based cell scaffolds.[29] The interdigitation fusion provides a method for preparing remarkably the single layer liposomes with exceptionally high internal volumes.[30] Increasing the concentration of diethylenetriaminepentaacetic acid in place of $CaCl^2$ in the process of making the scaffold can make the softened scaffold. In terms of tissue engineering, alginate is particularly attractive material because alginate gels, as well as favorable properties such as biocompatibility and ease of gelation, can be manipulated to maintain structural similarity with the extracellular matrix of the tissue and perform some important roles. Moreover, gold nanoparticles are also widely used in biology and medicine due to their

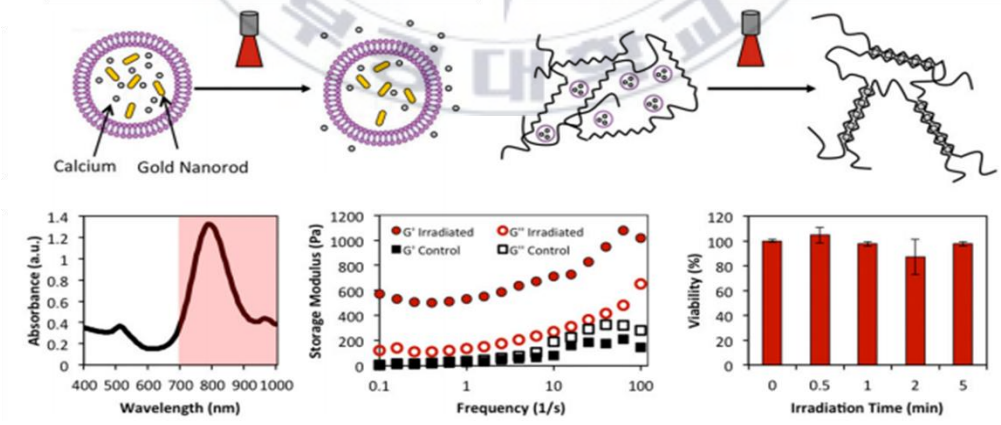

Figure 13. The mechanism and properties of the light-triggered release from temperature-sensitive liposome loaded with calcium and gold nanorods.[29]

wide range of chemical, physical properties and biocompatibility. When the prepared tissue-engineered scaffold is irradiated with near infrared rays, the gold nanoparticles generate heat to diffuse Ca^{2+} in the liposome, forming a scaffold as presented in Figure 12. In this study, cell scaffolds were fabricated by irradiating laser with 808 nm wavelength and 1.78 W/cm^2 output, and their viscoelastic characteristics were compared and analyzed by noninvasive measurement method and rheometer evaluation.

2.5. Rheometer measurement

In order to verify the validity of the proposed methods, the acoustic surface wave measurements of the scaffold and the rheometer (HR-2, TA Instruments, CA, USA) were compared and analyzed. Rheometer is instrument that measures viscosity and viscoelasticity of fluid, semisolids and solids using the relationship between strain, stress, and material deformation. Rheometer works by relating a materials property from how hard it's being pushed, to how far it moves by commanding stress and measuring strain or by commanding strain and measuring stress. A shear strain of 3% was applied at room temperature using an 8 mm parallel plate and the complex shear modulus of the scaffold was measured by applying an angular frequency of 0.1 rad/s to 10 rad/s.

Figure 14. The experimental setup of HR-2 TA Instruments rheometer.

2.6. Acoustic surface wave simulation

To confirm the possibility of measuring the elasticity of the cell scaffold, acoustic surface wave samples at different speeds were simulated. K-wave was used for scaffolds nonlinear behavioral simulation of sound. K-wave is Matlab-based acoustic simulation software and designed for the time-variant acoustic simulation of propagating ultrasonic waves in 1-dimension, 2-dimension, or 3-dimension.[31] The toolbox has a wide range of functionality applying various properties of transmitting, receiving, medium and boundary condition and advanced numerical model that can account for both linear and nonlinear wave propagation.[32] The simulation was divided into three main stages as shown in Figure 15. First, the total size of the medium to be computed for the ultrasonic wave propagation with the axial and lateral grid size

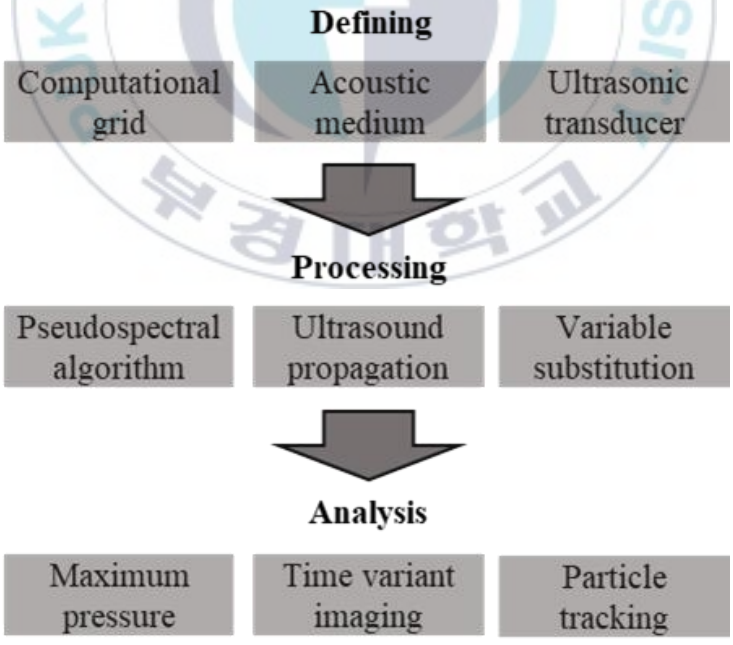

Figure 15. K-wave based ultrasonic simulation procedures

of 0.1 mm. Since then the characteristics of the medium and the properties of the transducer are determined. For the simulation, the acoustic absorption properties and density of the medium were calculated as homogeneous numerical values. Furthermore simulation was applied the values of K-wave viscoelastic and ultrasonic functions and derived the time-dependent results with Courant-Friedrichs-Lewy number 0.3.[33] Finally, based on the results obtained from each sample over time, the pressure and velocity are quantified and analyzed to confirm the possibility of acoustic surface wave measurement. Detailed simulation parameters are shown in Table 1.

Table 1 Simulation parameters

Source frequency	6.4 MHz
Source strength	800 kPa
Transmitting element	32
Receiving element	50
Pitch size	1 mm
Push duration	100 μs
Compression speed	1500 m/s
Absorption coefficient	0.0903 dB/(MHz·cm)

2.7. Acoustic surface wave measurement

In order to measure the acoustic surface wave velocity according to the change of the cell scaffold, the displacement of the acoustic surface wave was measured as shown in Figure 16. Ultrasound was focused under the surface of the cell scaffold for 600 μs from 128 elements of the transducer (L11-4v, Verasonics Inc., Kirkland, WA, USA) utilizing beam-forming for sufficient pushing on the scaffold surface. The resulting acoustic surface waves were received from 64 elements for 10 ms at a frame rate of 10 kHz using the ultrafast ultrasound imaging system (V-1, Verasonics Inc., Kirkland, WA, USA). Using the acquired data, the shear modulus was measured by calculating the

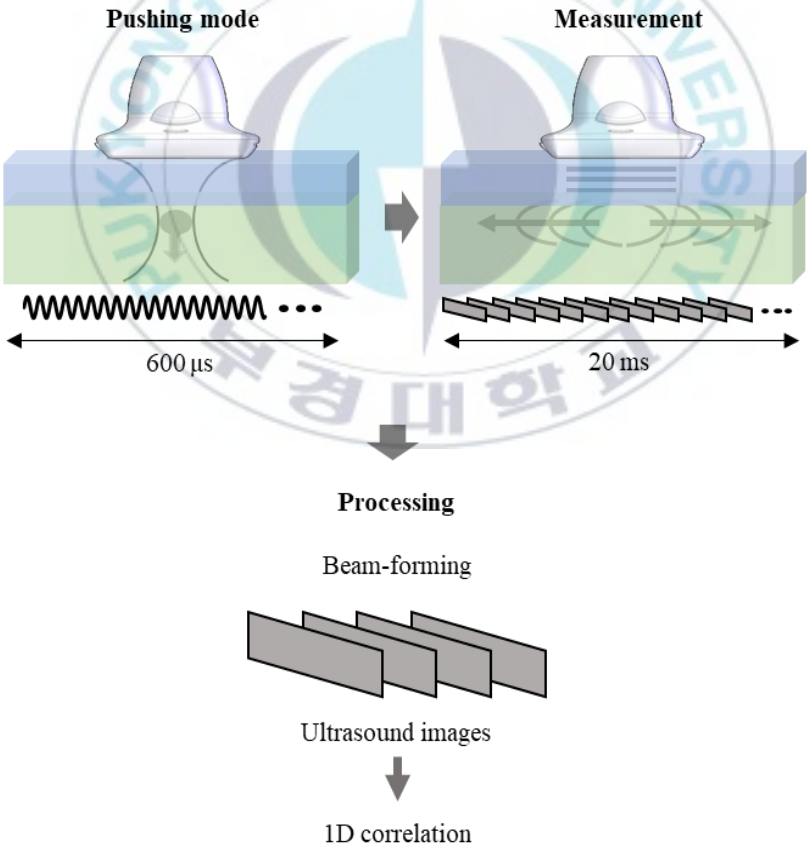

Figure 16. Acoustic surface wave measurement procedures.

Table 2 Experimental parameters for surface wave measurement

Source frequency	6.4 MHz
Source strength	800 kPa
Transmitting element	128
Receiving element	64
Pitch size	0.3 mm
Push duration	600 μs
Frame rate	10 kHz
Frame number	100

displacement at the surface with time and deriving the velocity of the acoustic surface wave. The experimental procedure is shown in Figure 16 and detailed experimental parameters are described in Table 2.

In this study, the measurement of the acoustic surface wave was carried out in the measurement range where the acoustic wave attenuation can sufficiently occur after the generation of the acoustic wave by the pushing. Also, since the displacement of the material due to acoustical radiation power is relatively small and the material is measured in a uniform and nearly isotropic condition, it can be interpreted by applying the assumption of a semi-infinite linear viscoelastic medium. Equations of linear viscoelastic media including these conditions can be derived as shown in Equation (3).[34]

$$(\lambda + 2\mu)\nabla(\nabla \cdot \mathbf{u}) - \mu\nabla^2\mathbf{u} = \rho\frac{\partial^2 \boldsymbol{u}}{\partial t^2} \qquad (3)$$

In equation (3), **u** is the displacement, ρ is the density, μ and λ are the lame coefficients associated with the transverse and longitudinal waves, respectively.[35] Since the elasticity measurements carried out in this study are due only to transverse waves, the components of the longitudinal wave associated with the bulk modulus can be expressed as (4) by excluding from equation (3).

$$\mu\nabla^2\mathbf{u} = \rho\frac{\partial^2\boldsymbol{u}}{\partial t^2} \quad (4)$$

Also, the displacement of the medium due to pushing exists mainly in the axial direction, and it can be summarized as equation (5) according to the propagation direction and acoustic frequency of the transverse wave.

$$U_z(r,\omega) = a(\omega)\frac{i}{4}H_0^1(k_s(\omega)r) \quad (5)$$

In equation (5), ω is the angular frequency, $a(\omega)$ is the amplitude according to the angular frequency, r is the distance from the transverse wave generating point, H_0^1 is the Hankel function and $k^*(\omega)$ is the complex shear wave number and it can be expressed as $k^*(\omega) = k_r - ik_i$.

$$G^*(\omega) = G'(\omega)+iG''(\omega) \quad (6)$$

On the other hand, the complex shear modulus can be expressed as equation 6, which is composed of G' storage modulus and G'' loss modulus in a linear viscoelastic medium.

$$G^*(\omega) = \frac{\rho\omega^2}{k^*(\omega)^2} \quad (7)$$

The storage elastic modulus, loss elastic modulus, and loss tangent are summarized as follows using equation (7).

$$G'(\omega) = \rho\omega^2 \frac{k_r^2 - k_i^2}{k_r^2 + k_i^2} \quad (8)$$

$$G''(\omega) = -2\rho\omega^2 \frac{k_r k_i}{k_r^2 + k_i^2} \quad (9)$$

$$\tan\delta(\omega) = \frac{G''}{G'} = \frac{2k_r k_i}{k_r^2 - k_i^2} \quad (10)$$

The shear wave velocity can be calculated from equation (9) by applying poisson's ratio from the velocity of the measured acoustic surface wave, and the storage modulus can be measured by applying equation (10).

3. Results

3.1. Particle velocity maps of superficial tissue engineering models

In order to monitor the effects of the acoustic surface waves on SWEI in the superficial regions, the particle velocities were compared at various time points (1 ms, 2 ms, 3 ms, and 4 ms). The particle velocity maps were the result of 2-dimensional autocorrelation from the B-mode images over time. The B-mode image was also compounded at three angles after applying absolute value, log scale, and dynamic range from acquired IQ data using ultrafast ultrasound system. In Figure 17(a), it was shown that the acoustic surface wave and the shear wave were located at similar lateral positions until 1 ms from the end of the acoustic radiation force. However, due to differences in the propagation speed and the signal intensity of the surface and shear waves, spatial separation between the two waves occurred in the particle velocity maps in Figures 17(b-d). Since the strong ultrasonic signals from the surface can interfere with shear wave propagation, it can degrade the accuracy of shear modulus measurement and limit the imaging capabilities of SWEI.

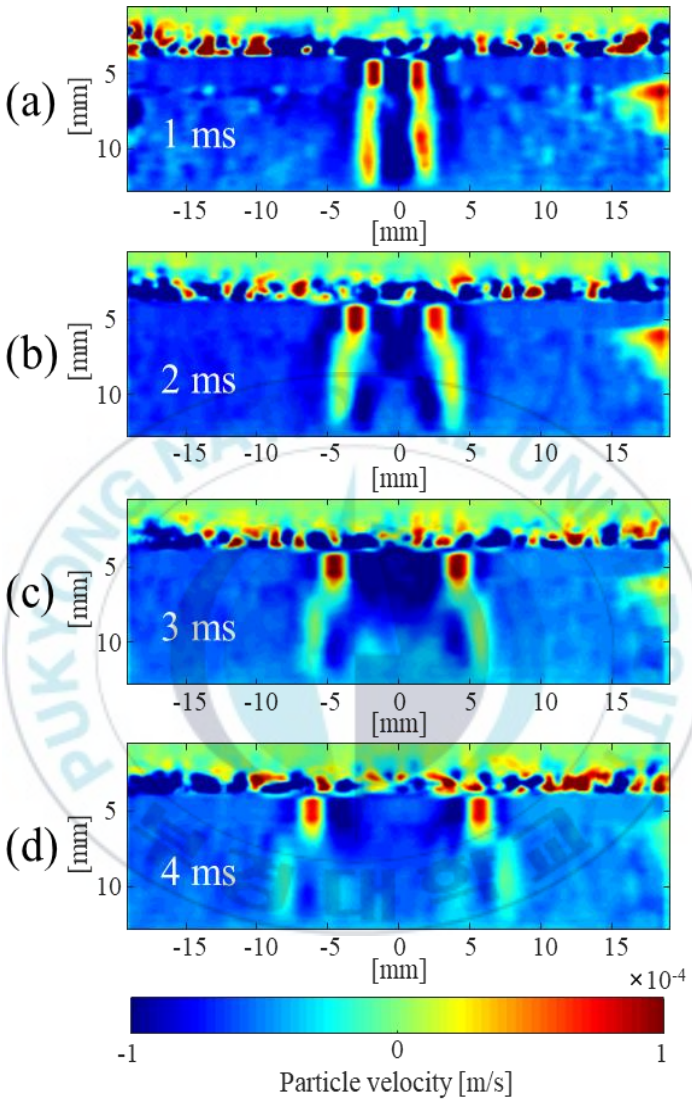

Figure 17. Particle velocity maps after ultrasonic pushing at various time points of (a) 1 ms, (b) 2 ms, (c) 3 ms and (d) 4ms.

3.2. Optimization of cross-correlation for SWEI in superficial regions

To alleviate the quantification errors in the superficial regions, shear moduli were evaluated with various window sizes (2, 4, 6, and 8) when calculating cross-correlation. The shear moduli were estimated with four different region of interests (ROIs) to compare the interferences of acoustic surface waves at different lateral and axial locations as shown in Figure 18. When the window size was considerably small as presented in Figure 18(a), the estimation of the shear modulus resulted in the incorrect values, which are significantly lower than the nominal values because the window size could be too small to scan the particle velocity map. When applying the windows sizes of 6 and 8, substantial artifacts in the shear moduli maps were observed in Figures 18(c) and 18(d), because the larger window sizes may have increased the unwanted effects of the acoustic surface waves. In our study, the lowest errors were occurred with the window size of 4 as presented in Figure 18(b).

Statistical analysis was applied to the post-processed data using box whisker plots for each ROI as shown in Figure 19. Overall, the shear moduli in the upper regions of ROIs were less accurately assessed with higher variance and more outliers and were affected by the acoustic surface waves compared to those in the lower regions. As described in the results in Figure 18(a), statistical analysis with window size 2 in Figure 19 indicates that it is too small to accurately assess the shear modulus. Also, the shear moduli estimated with window size 6 and 8 showed higher variations compared to those with window size 4, which may imply that the acoustic surface wave can deteriorate the accuracy of SWEI in the superficial tissue regions and optimization of window size in SWEI is essential.

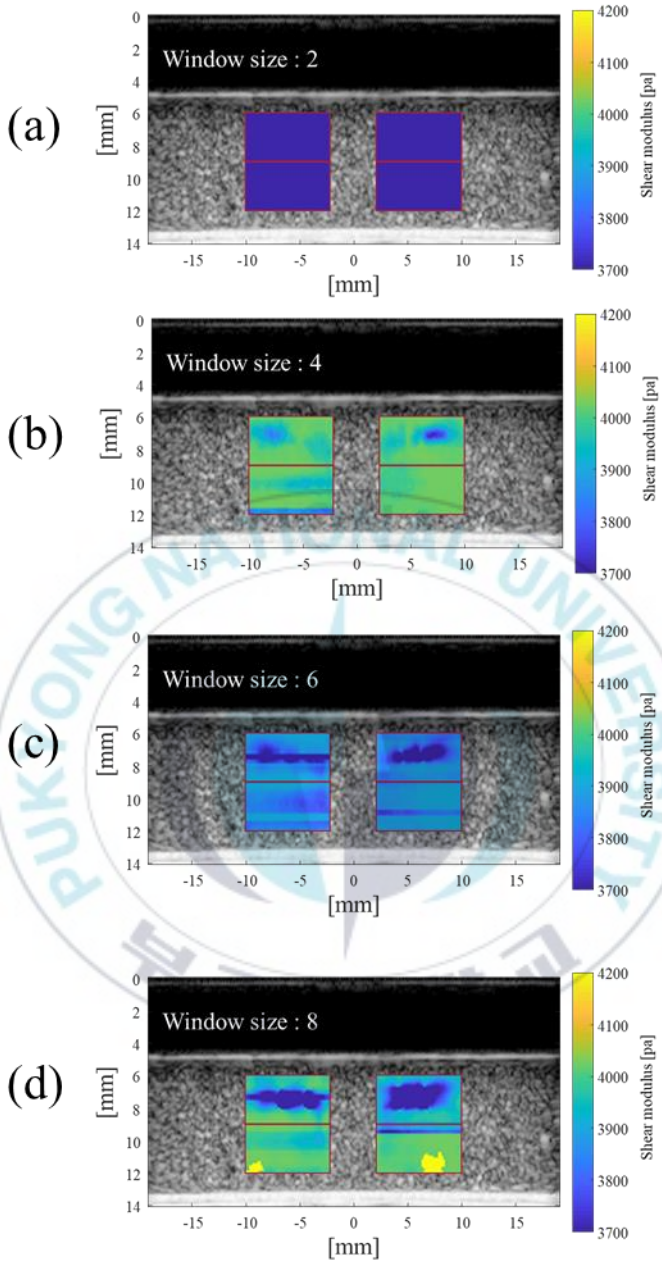

Figure 18. Shear wave elasticity imaging in four regions of interest using different cross-correlation window sizes of (a) 2, (b) 4, (c) 6 and (d) 8.

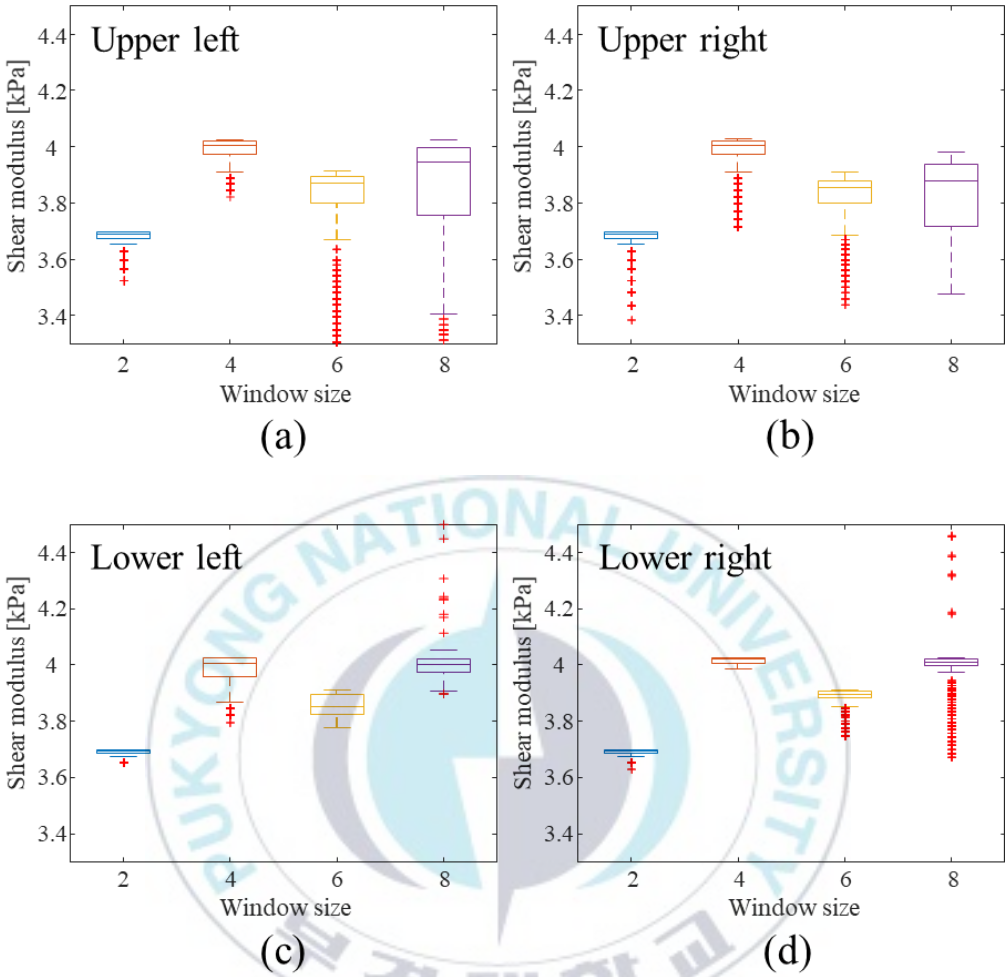

Figure 19. Shear moduli represented using box whisker plots in four regions of interest ((a) upper left, (b) upper right, (c) lower left, and (d) lower right).

3.3. Simulation of acoustic surface wave

The K-wave was simulated by applying the Table 1 values in the size of 51.2 mm × 51.2 mm media. The K-wave is a matlab-based tool that can perform acoustical calculations on viscoelastic medium in a variety of dimensions over time. The source frequency and source strength applied in the simulation was based on the numerical parameters of the transducer (L11-4v, Verasonics, Inc.) and the procedure of acoustic surface wave imaging also used in the actual ultrasound data acquisition parameters. Furthermore, the numerical values of the acoustic surface wave simulation were optimized to tissue engineering applications.

Four different viscoelastic properties were applied to measure the particle velocities and pressures of the acoustic surface wave simulations over time. The speeds of 10 m/s, 20 m/s, 30 m/s and 40 m/s used in the simulation were derived from parameters of tissue engineering scaffold measured with rheometer and converted to parameters suitable for acoustic simulation. Additionally, changing of acoustic intensity as time was shown using the calculation from particle velocities and pressures. The Figures 20(a-d) shows the change in acoustic intensity over time in different samples (a) 10 m/s, (b) 20 m/s, (c) 30 m/s and (d) 40 m/s, which means the progression of acoustic surface waves. In order to confirm the propagation of the acoustic surface wave, the slope was confirmed by plotting the acoustic intensity with time on the surface of the simulated medium. As shown in Figure 20(a), the acoustic intensity changes little according to the time, and in Figure 20(d), it can see that acoustic intensity changes rapidly according to the time. It was confirmed by simulation that the acoustic surface waves travel faster as the viscoelastic material changes from 10 m/s to 40 m/s.

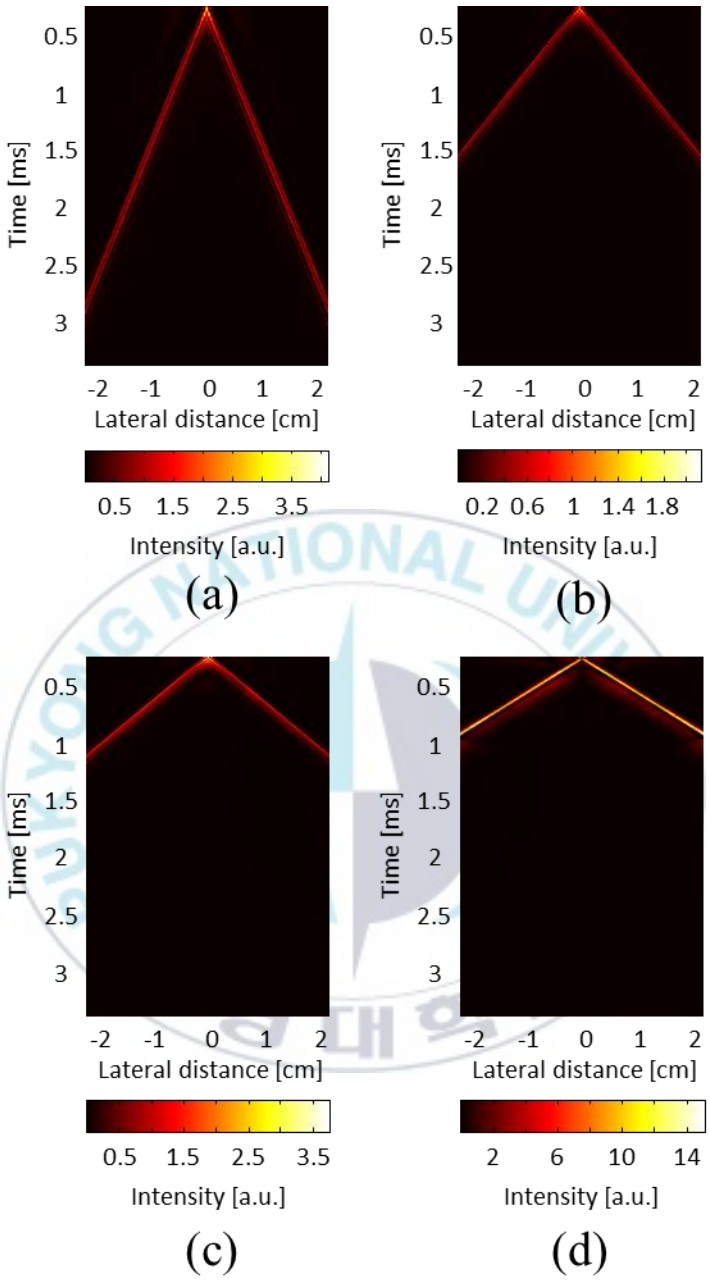

Figure 20. Simulation of surface wave propagation speeds at different reference mechanical properties of (a) 10 m/s, (b) 20 m/s, (c) 30 m/s and (d) 40 m/s.

Accordingly the velocity of the acoustic surface wave was quantified using the slope of the propagation velocity with time, and then compared with the reference value. As shown in Figure 21, when comparing the measured values from the rheometer and the derived acoustic surface wave speed by applying the simulations, the same trend was shown and it was confirmed that the numerical value of the simulation was somewhat low. In conclusion, the measurement of the mechanical properties of the tissue engineering scaffold was possible using acoustic surface waves, although the simulation showed some differences because it does not include all the characteristics of the acoustic non-linearity.

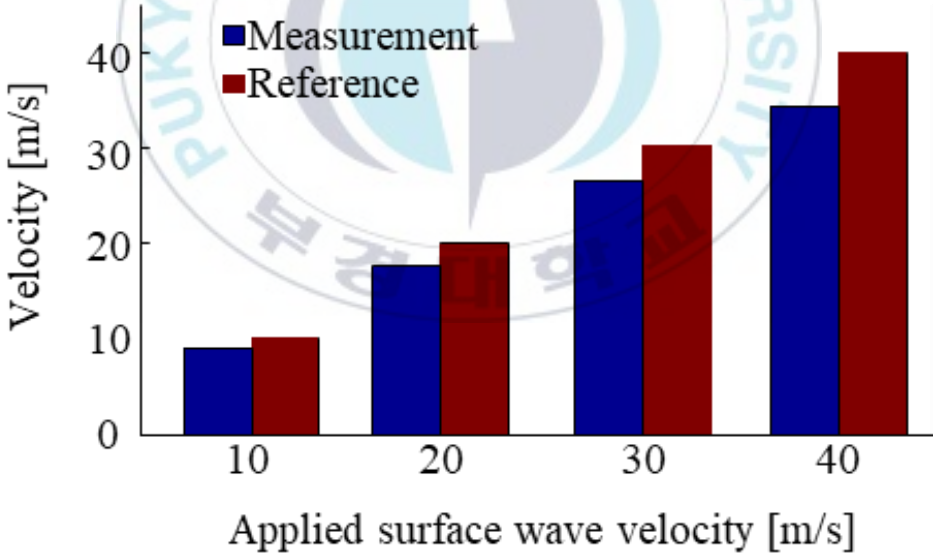

Figure 21. Simulated and reference surface wave velocities at different mechanical properties.

3.4. Acoustic surface wave measurement

Shear moduli of 3%, 6%, 9% and 12% gelatin based scaffolds were measured and compared using acoustic surface wave method and rheometer. The acoustic surface wave was measured using an ultrafast imaging system and the ultrasound was focused under the 80 wavelength of the scaffolds surface. It is a consideration of errors due to displacement of the tissue-engineered scaffolds surface when exciting a long pulse using the F-number for sufficient acoustic radiation force. Ultrasound B-mode images were acquired through post-processing after acquiring 100 frames of IQ data at 10 kHz frame rate. In addition, cross-correlation and 2D autocorrelation were performed by upsampling using the mathematical interpolation techniques to track accurate surface wave propagation. The propagation images of surface wave was described the displacement on the surface according to the time in order to indicate that the surface wave is progressing both way on the surface of tissue-engineered scaffolds. The experimental setup parameters are shown in Table 2.

Displacements of acoustic surface wave analyze the received data and shows the changing of displacement over time at 100 μs intervals. In Figure 22, the slope of the maximum point of displacement moving with time was measured differently according to the gelatin concentration of (a) 3%, (b) 6%, (c) 9% and (d) 12 % for various tissue engineering mechanical properties. The temporal shift of the displacement was faster in more stiffness materials as the results shown in the simulation of acoustic surface wave, which means the progression of the acoustic surface wave also faster as shown in Figure 22. In summary, acoustic surface waves can be measured at various gelatin concentrations, and as the gelatin concentration increases, acoustic surface waves move rapidly.

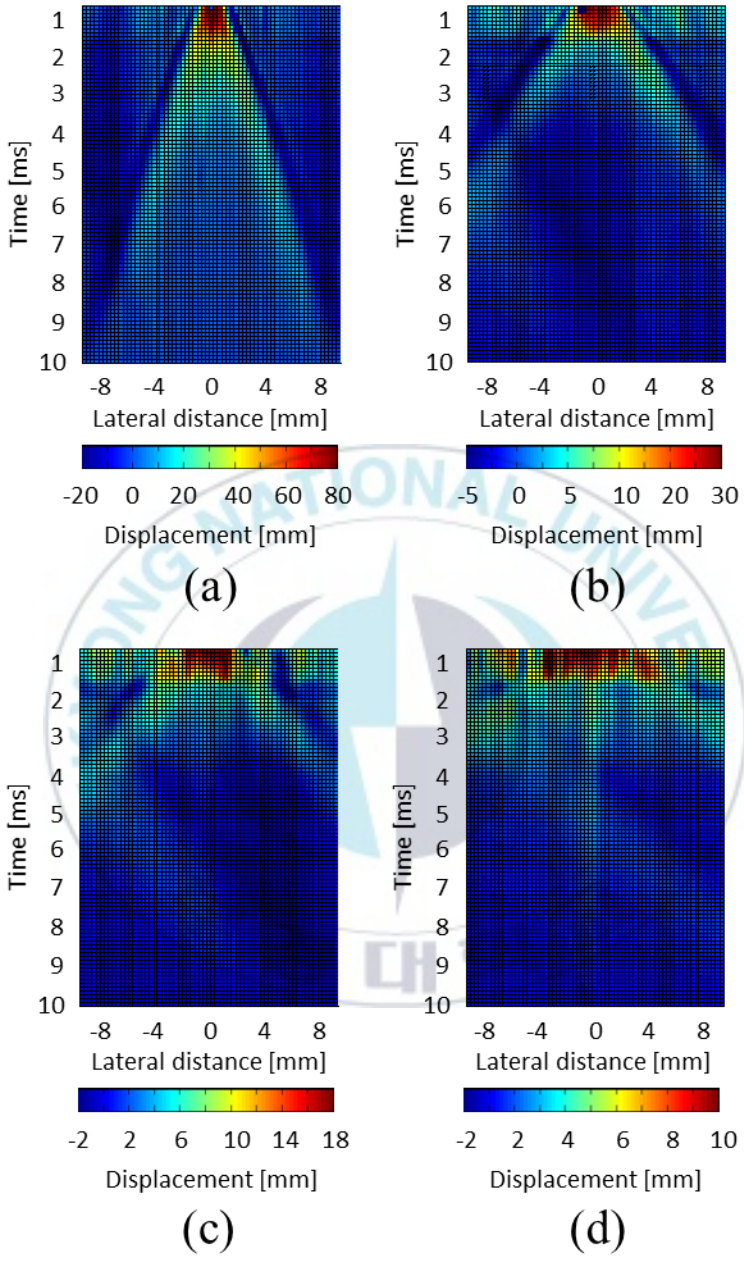

Figure 22. Evaluation of surface wave propagation at different mechanical properties of (a) 3%, (b) 6%, (c) 9% and (d) 12% gelatin phantom.

To verify the validity of the acoustic surface wave measurement, the acoustic surface wave displacement measured in Figure 22 was calculated as the shear modulus and compared with the rheometer measurement and quantified through the bar graph as shown in Figure 23. Except for the concentration of 12% gelatin scaffold, the values of shear modulus measured using acoustic surface wave and rheometer were similar, though surface wave measurements were slightly larger than those measured by rheometer. The error at the concentration of 12% gelatin scaffold seems to be due to the low SNR and the lack of acoustic radiation intensity compared to the high viscoelasticity.

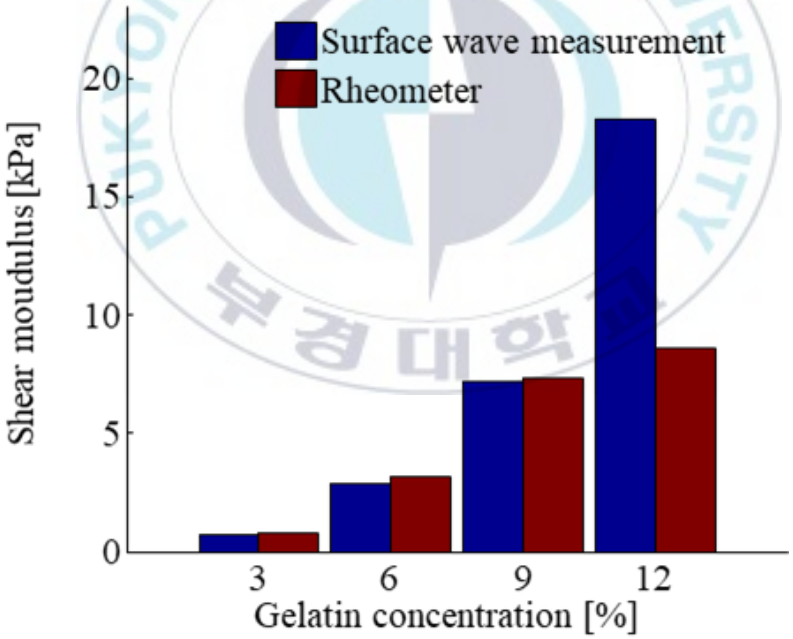

Figure 23. Shear moduli assessed by surface wave measurement and rheometer at different gelatin concentrations.

In order to investigate the possibility of non-destructive viscoelasticity measurement of tissue-engineered scaffolds which are frequently applied to tissue engineering, alginate gold nanoparticle based cell scaffolds were measured the acoustic surface wave and mechanical property. In order to remove the artifact caused by the ultrasonic reverberation, the PVA phantom for ultrasonic absorption was placed at the bottom of the cell scaffold. In Figure 24, the red arrow is the position where acoustic radiation force is applied to generate the surface wave on the tissue-engineered scaffold, and the yellow arrow is tracking according to the time after the surface wave is generated. No acoustic scattering material was added to the scaffold, ultrasonic reflection signals were observed only on the scaffold surface as shown in Figures 24(a-d). Furthermore, Figures 24(a-d) can be seen to progress through acoustic surface waves when viewed at (a) 2 ms, (b) 3 ms, (c) 4 ms, and (d) 5 ms. Figure 25(a) shows the propagation of the surface wave over time up to 10 ms at 100 μs interval time through the displacement map. The displacement with time is also confirmed that the measuring shear modulus value(0.2348 kPa) applying the evaluation of acoustic surface wave is similar to the measurement value(0.2420 kPa) using rheometer as shown in Figure 25(b).

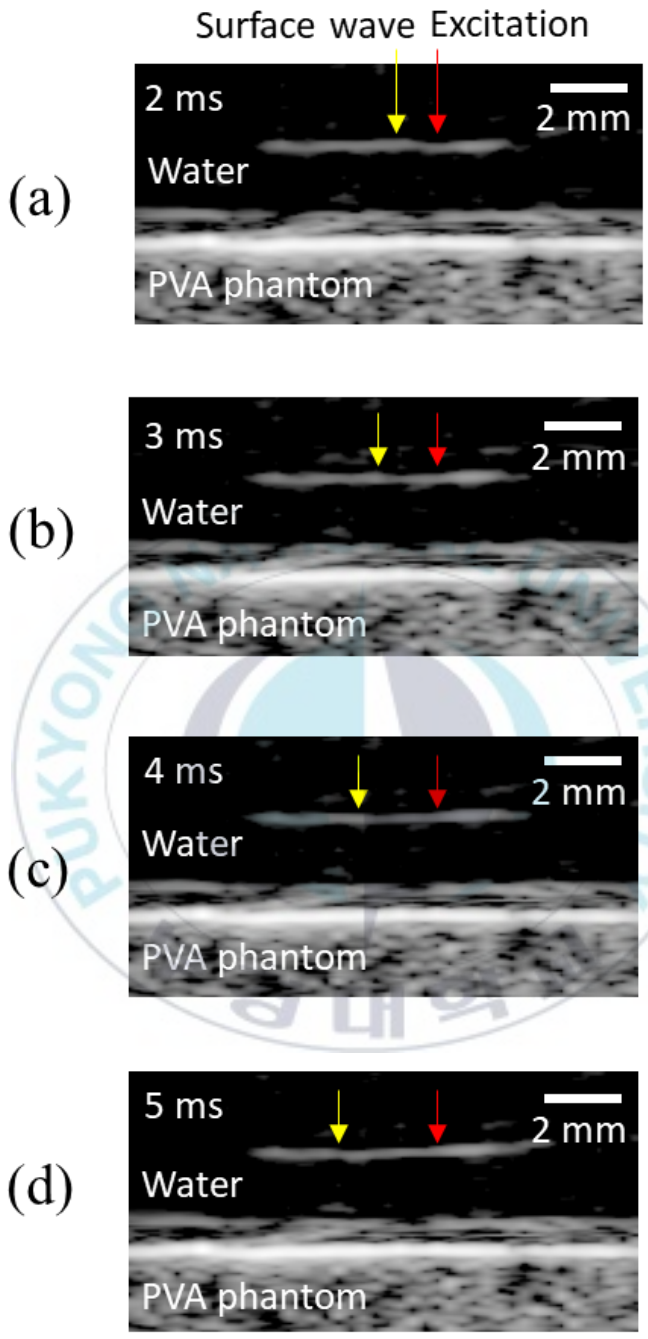

Figure 24. Surface wave propagation in B-mode images of alginate-gold nanoparticle based tissue-engineered scaffolds different time points of (a) 2 ms, (b) 3 ms, (c) 4 ms and (d) 5 ms.

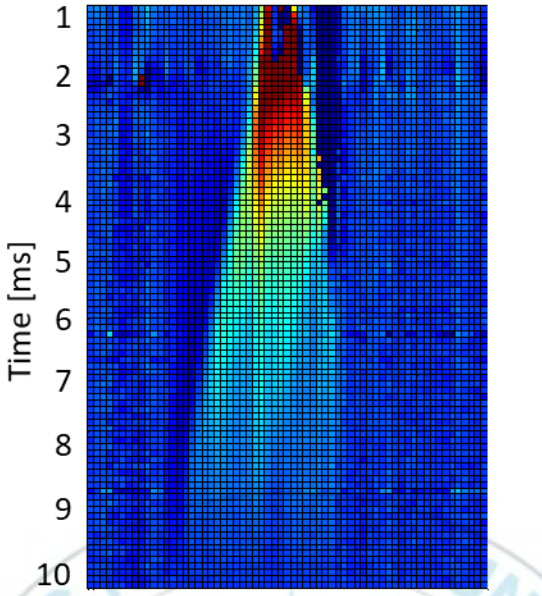

(a)

Shear modulus [kPa]	
Surface wave measurement	Rheometer
0.2348	0.2420

(b)

Figure 25. (a) Measurement of surface wave propagation in alginate-gold nanoparticle based tissue-engineered scaffolds. (b) Shear moduli assessed by surface wave measurement and rheometer.

4. Discussion

Recently, many studies have explored diverse applications of SWEI to quantitatively and non-destructively monitor the mechanical properties of tissue-engineered constructs.[8] Typically, a depth of tissue engineered constructs or transplantation is less than a few centimeters, so various tissue engineering applications can be performed in the superficial tissue regions.[20] This study investigated the effect of the acoustic surface wave on the assessment of the shear moduli in the superficial regions as a function of window size of cross-correlation in SWEI. It was demonstrated that data processing in SWEI is essential because the accuracy and reliability of the assessment of mechanical properties depend on the processing parameters. To guarantee the detection accuracy and minimize the errors resulting from the acoustic surface waves during the data processing, a role of the cross-correlation window size is essential and needs to be optimized. In this study, the most accurate experimental results were obtained with window size 4, but this window size would likely vary because of other reasons, such as shear wavelength and tissue stiffness. Moreover, using the suggested method, the acoustic surface wave speed also can be calculated by applying the Poisson's ratio, which can be used to compensate and enhance the assessment of the shear modulus of the constructs. Also, in addition to the window sizes, other parameters or algorithms in the post-processing such as novel beamforming and harmonic autocorrelation can be further considered to enhance the shear modulus assessment in the superficial regions.[27] Furthermore, SWEI is currently most commonly used to estimate shear wave propagation speed at multiple tracking locations by transmitting one push beam to measure shear wave propagation speed.[36] However, multiple

tracking location approach is based on the assumption that the tracking place is in the middle of push beam and the speckle of the point to estimate is different, causing shearing and causing errors.[37] In order to reduce these errors, there is a method of compounding at various angles by dual phase transmit focusing.[18] However, in the case of tissue engineering applications, the depth is so short that it cannot be applied without additional devices such as a gel pad which can change and attenuate acoustic characteristics.[38] However, by improving the transducer, sequence and specification of the current ultrasound imaging system, if SWEI multi focusing by pushing the shear wave propagation speed at one point in several places of one transducer, the shear modulus will be tracking the single location and the same speckle, it seems that these errors can be reduced.[37, 39] Acoustic surface waves are a non-destructive and non-invasive method of measuring physical properties without any scattering material in tissue engineering.[40] In this nondestructive testing and engineering field, simulation is an inevitable process before measurement. Simulations in 3D structures with such viscoelastic properties have been performed through COMSOL or Matlab-based Febio or K-wave.[41, 42] In this paper, simulation have been applied the necessary parameters for viscoelastic medium using K-wave that can perform acoustical calculations on viscoelastic medium in various dimensions over time. However, applying more boundary and initial conditions, further segmenting the time and reducing the grid size to the simulation can take more time but yield less error results through simulation. The error in the 12% gelatin phantom is due to the low SNR due to the low acoustical radiation intensity compared to the high viscoelasticity. Therefore, increasing the pulse duration to increase the acoustical radiation force, increasing the transducer voltage or excitation elements, and using the high intensity focused

ultrasound (HIFU) transducer is expected to improve these limitations.[43] Also, based on push location in alginate-gold nanoparticle based tissue-engineered scaffold, the surface wave in the left part was tracked, but the surface wave in the right part was not tracked. However, as shown in Figure 24, this error is due to the pushing area to the right of the alginate-gold nanoparticle based tissue-engineered scaffold. Therefore, the opposite shear modulus can also be measured by acoustic surface waves after pushing to the left through beamforming.

5. Conclusion

In conclusion, the shear moduli were measured in the superficial regions of the tissue-mimicking model using SWEI, and the experimental results indicate that quantification errors caused by interference of acoustic surface waves were observed. To minimize the inaccuracies, data processing related to cross-correlation was optimized for precise assessment of shear wave propagation speeds. This study applied different window sizes when calculating cross-correlation and comparing the quality of data processing. Also, the results were statistically analyzed in four different ROIs in the phantom using the box whisker plots. As a result, it was demonstrated that detection accuracy decreased when the window size of cross-correlation became small, and the interference of the acoustic surface wave increased when the window size of cross-correlation became larger, respectively. Therefore, it is desirable to optimize parameters for the assessments of the shear moduli in the superficial regions for tissue engineering applications. Also, this study can be further extended to diverse preclinical and clinical approaches. In addition, this study confirmed the possibility of quantitative measurement of tissue-engineered scaffolds using simulation and acoustic surface wave using the ultrafast ultrasound imaging system. Simulation results show that the acoustic surface wave velocity changes with the change of mechanical properties, which is similar to the actual acoustic surface wave measurements performed on 4 different concentration of the gelatin based scaffolds and dynamic phototuning alginate-gold nanoparticle based cell scaffolds. Also, the validity of the acoustic surface wave method was verified by comparing measurements of shear modulus derived from acoustic surface wave measurements and measurements of shear modulus measured

with a rheometer. In conclusion, non-destructive and non-invasive characterization and validation of acoustic surface wave measurements were verified through various tissue engineering applications and simulations. In addition, the measurement of the mechanical property using the acoustic surface wave can be extended to a variety of preclinical and clinical approaches, including tissue engineering and biomedical applications.

6. References

[1] Ma, L., C. Gao, Z. Mao, J. Zhou, J. Shen, X. Hu and C. Han (2003). "Collagen/chitosan porous scaffolds with improved biostability for skin tissue engineering." Biomaterials **24**(26): 4833-4841.

[2] Khademhosseini, A. and R. Langer (2016). "A decade of progress in tissue engineering." Nature protocols **11**(10): 1775.

[3] O'brien, F. J. (2011). "Biomaterials & scaffolds for tissue engineering." Materials today **14**(3): 88-95.

[4] Baker, S. C., G. Rohman, J. Southgate and N. R. Cameron (2009). "The relationship between the mechanical properties and cell behaviour on PLGA and PCL scaffolds for bladder tissue engineering." Biomaterials **30**(7): 1321-1328.

[5] Kim, M. H., C. Yun, E. P. Chalisserry, Y. W. Lee, H. W. Kang, S.-H. Park, W.-K. Jung, J. Oh and S. Y. Nam (2018). "Quantitative analysis of the role of nanohydroxyapatite (nHA) on 3D-printed PCL/nHA composite scaffolds." Materials Letters **220**: 112-115.

[6] Tran, T., Z. Hamid and K. Cheong (2018). A Review of Mechanical Properties of Scaffold in Tissue Engineering: Aloe Vera Composites. Journal of Physics: Conference Series, IOP Publishing.

[7] Parajuli, R. K., N. Sunaguchi, R. Tei, T. Iijima and Y. Yamakoshi (2014). "Characterization of nonlinearity of shear elasticity using local velocity mapping." Japanese Journal of Applied Physics **53**(7S): 07KF30.

[8] Kim, K. and W. R. Wagner (2016). "Non-invasive and non-destructive characterization of tissue engineered constructs using ultrasound imaging technologies: a review." Annals of Biomedical Engineering **44**(3): 621-635.

[9] Kuo, P.-L., C.-C. Charng, P.-C. Wu and P.-C. Li (2017). "Shear-wave elasticity measurements of three-dimensional cell cultures for mechanobiology." Journal of Cell Science **130**(1): 292-302.

[10] Choi, Y. S., S. R. Hong, Y. M. Lee, K. W. Song, M. H. Park and Y. S. Nam (1999). "Study on gelatin-containing artificial skin: I. Preparation and characteristics of novel gelatin-alginate sponge." Biomaterials **20**(5): 409-417.

[11] Wang, X., Q. Ao, X. Tian, J. Fan, H. Tong, W. Hou and S. Bai (2017). "Gelatin-based hydrogels for organ 3D bioprinting." Polymers **9**(9): 401.

[12] Sela, M. and R. Arnon (1960). "Studies on the chemical basis of the antigenicity of proteins. 1. Antigenicity of polypeptidyl gelatins." Biochemical Journal **75**(1): 91.

[13] Lu, H., H. H. Oh, N. Kawazoe, K. Yamagishi and G. Chen (2012). "PLLA–collagen and PLLA–gelatin hybrid scaffolds with funnel-like porous structure for skin tissue engineering." Science and technology of advanced materials **13**(6): 064210.

[14] Ma, P. X. (2008). "Biomimetic materials for tissue engineering." Advanced drug delivery reviews **60**(2): 184-198.

[15] Deng, Y., N. C. Rouze, M. L. Palmeri and K. R. Nightingale (2017). "Ultrasonic shear wave elasticity imaging sequencing and data processing using a verasonics research scanner." IEEE transactions on ultrasonics, ferroelectrics, and frequency control **64**(1): 164-176.

[16] Wang, L. (2018). "Acoustic radiation force based ultrasound elasticity imaging for biomedical applications." Sensors **18**(7): 2252.

[17] Sigrist, R. M., J. Liau, A. El Kaffas, M. C. Chammas and J. K. Willmann (2017). "Ultrasound elastography: review of techniques and clinical applications." Theranostics **7**(5): 1303.

[18] Yoon, H., S. R. Aglyamov and S. Y. Emelianov (2017). "Dual-Phase Transmit Focusing for Multiangle Compound Shear-Wave Elasticity Imaging." IEEE transactions on ultrasonics, ferroelectrics, and frequency control **64**(10): 1439-1449.

[19] Bhatia, K. S., C. C. Cho, C. S. Tong, E. H. Yuen and A. T. Ahuja (2012). "Shear wave elasticity imaging of cervical lymph nodes." Ultrasound in medicine & biology **38**(2): 195-201.

[20] Bude, R. O. and R. S. Adler (1995). "An easily made, low-cost, tissue-like ultrasound phantom material." Journal of clinical ultrasound **23**(4): 271-273.

[21] Zhang, X., B. Qiang, R. Hubmayr, M. Urban, R. Kinnick and J. Greenleaf (2011). "Noninvasive ultrasound image guided surface wave method for measuring the wave speed and estimating the elasticity of lungs: A feasibility study." Ultrasonics **51**(3): 289-295.

[22] Schmitt, J. M. and G. Kumar (1998). "Optical scattering properties of soft tissue: a discrete particle model." Applied optics **37**(13): 2788-2797.

[23] Zhang, X., B. Qiang and J. Greenleaf (2011). "Comparison of the surface wave method and the indentation method for measuring the elasticity of gelatin phantoms of different concentrations." Ultrasonics **51**(2): 157-164.

[24] Liu, Y., J. Liu, B. Z. Fite, J. Foiret, A. Ilovitsh, J. K. Leach, E. Dumont, C. F. Caskey and K. W. Ferrara (2017). "Supersonic transient magnetic resonance elastography for quantitative assessment of tissue elasticity." Physics in Medicine & Biology **62**(10): 4083.

[25] Jeong, W. K., H. K. Lim, H.-K. Lee, J. M. Jo and Y. Kim (2014). "Principles and clinical application of ultrasound elastography for diffuse liver disease." Ultrasonography **33**(3): 149.

[26] Ophir, J., I. Cespedes, H. Ponnekanti, Y. Yazdi and X. Li (1991). "Elastography: a quantitative method for imaging the elasticity of biological tissues." Ultrasonic imaging **13**(2): 111-134.

[27] Amador, C., P. Song, D. D. Meixner, S. Chen and M. W. Urban (2016). "Improvement of shear wave motion detection using harmonic imaging in healthy human liver." Ultrasound in medicine & biology **42**(5): 1031-1041.

[28] Song, P., A. Manduca, H. Zhao, M. W. Urban, J. F. Greenleaf and S. Chen (2014). "Fast shear compounding using robust 2-D shear wave speed calculation and multi-directional filtering." Ultrasound in medicine & biology **40**(6): 1343-1355.

[29] Stowers, R. S., S. C. Allen and L. J. Suggs (2015). "Dynamic phototuning of 3D hydrogel stiffness." Proceedings of the National Academy of Sciences **112**(7): 1953-1958.

[30] Ahl, P. L., L. Chen, W. R. Perkins, S. R. Minchey, L. T. Boni, T. F. Taraschi and A. S. Janoff (1994). "Interdigitation-fusion: a new method for producing lipid vesicles of high internal volume." Biochimica et Biophysica Acta (BBA)-Biomembranes **1195**(2): 237-244.

[31] Treeby, B. E. and B. T. Cox (2010). "k-Wave: MATLAB toolbox for the simulation and reconstruction of photoacoustic wave fields." Journal of biomedical optics **15**(2): 021314.

[32] Treeby, B. E., J. Jaros, A. P. Rendell and B. Cox (2012). "Modeling nonlinear ultrasound propagation in heterogeneous media with power law absorption using ak-

space pseudospectral method." The Journal of the Acoustical Society of America **131**(6): 4324-4336.

[33] Batycky, R., M. J. Blunt and M. R. Thiele (1997). "A 3D field-scale streamline-based reservoir simulator." SPE Reservoir Engineering **12**(04): 246-254.

[34] Miller, G. and H. Pursey (1954). "The field and radiation impedance of mechanical radiators on the free surface of a semi-infinite isotropic solid." Proc. R. Soc. Lond. A **223**(1155): 521-541.

[35] Zhang, X. and J. F. Greenleaf (2007). "Estimation of tissue's elasticity with surface wave speed." The Journal of the Acoustical Society of America **122**(5): 2522-2525.

[36] McAleavey, S., E. Collins, J. Kelly, E. Elegbe and M. Menon (2009). "Validation of SMURF estimation of shear modulus in hydrogels." Ultrasonic imaging **31**(2): 131-150.

[37] Elegbe, E. C. and S. A. McAleavey (2013). "Single tracking location methods suppress speckle noise in shear wave velocity estimation." Ultrasonic imaging **35**(2): 109-125.

[38] Klucinec, B. (1996). "The effectiveness of the Aquaflex gel pad in the transmission of acoustic energy." Journal of athletic training **31**(4): 313.

[39] Kim, B.-H., G.-D. Kim and T.-K. Song (2007). "A post-compression based ultrasound imaging technique for simultaneous transmit multi-zone focusing." Ultrasonics **46**(2): 148-154.

[40] Sarvazyan, A. P., M. W. Urban and J. F. Greenleaf (2013). "Acoustic waves in medical imaging and diagnostics." Ultrasound in medicine & biology **39**(7): 1133-1146.

[41] Audière, S., E. D. Angelini, L. Sandrin and M. Charbit (2014). "Maximum likelihood estimation of shear wave speed in transient elastography." IEEE transactions on medical imaging **33**(6): 1338-1349.

[42] Wang, Y., E. Helminen and J. Jiang (2015). "Building a virtual simulation platform for quasistatic breast ultrasound elastography using open source software: A preliminary investigation." Medical physics **42**(9): 5453-5466.

[43] Iwasaki, R., R. Takagi, R. Nagaoka, H. Jimbo, S. Yoshizawa, Y. Saijo and S.-i. Umemura (2016). "Monitoring of high-intensity focused ultrasound treatment by shear wave elastography induced by two-dimensional-array therapeutic transducer." Japanese Journal of Applied Physics **55**(7S1): 07KF05.